scientific reports

Check for updates

OPEN

Human neural rosettes secrete bioactive extracellular vesicles enriched in neuronal and glial cellular components

Malena Herrera Lopez[1,2], Matías Bertone Arolfo[1,2], Mónica Remedi[1], Laura Gastaldi[1], Carlos Wilson[1], Gonzalo G. Guendulain[1], Danilo Ceschin[1], Andrés Cardozo Gizzi[1], Alfredo Cáceres[1]✉ & Ana Lis Moyano[1]✉

Extracellular vesicles (EVs) play a critical role in the development of neural cells in the central nervous system (CNS). Human neural rosettes (hNRs) are radial cell structures that assemble from induced pluripotent stem cells (hiPSCs) and recapitulate some stages of neural tube morphogenesis. Here we show that hiPSCs and hNRs secrete EVs (hiPSC-EVs and hNR-EVs) with distinctive protein cargoes. Remarkably, hNR-EVs carry neuronal and glial cellular components involved in human CNS development. Importantly, hNR-EVs stimulate stem cells to change their cellular morphology and promote neurite growth in human and murine neurons with a significant dysregulation of SOX2 levels. This transcription factor modulates both neural differentiation and pluripotency. Interestingly, these effects were inhibited by antibodies against an unexpected neuroglial cargo of hNR-EVs: the major proteolipid protein (PLP). These findings show that hNRs secrete bioactive EVs containing neural components and might contribute as trophic factors during human neurodevelopment.

Keywords CNS, Neurodevelopment, Extracellular vesicles, Stem cells, Neurite outgrowth, SOX2, PLP, Myelin

Human neural rosettes (hNRs) are an assembly of neural cells generated *in vitro* from induced pluripotent stem cells (hiPSCs). These radial structures exhibit apicobasal polarity, resembling the cellular architecture of the human neural tube. hNRs generate neurons and glial cells of the central nervous system (CNS) recapitulating key molecular and biological events associated with human brain morphogenesis and development[1,2]. hNRs exhibit a heterogeneous population of cells including neuroepithelial, neural stem and progenitor cells that potentially can differentiate into any CNS cell type. Therefore, hNRs are a promising *in vitro* model to study human neurodevelopment[3].

Several trophic factors are used to maintain hNRs *in vitro* but little is known about the secreted cellular components that may contribute to spatiotemporal coordination of hNRs formation. Extracellular vesicles (EVs) are nanosized vesicles that transport lipids, proteins and nucleic acids among different CNS cell types and their cargoes can elicit a phenotypic response in acceptor cells[4,5]. EVs secreted in CNS development might regulate proliferation and differentiation of stem and progenitor cells essential for neural growth and localization[6,7]. However, little is known about EVs biology, their cargoes and biological significance during fetal development of the human CNS.

Neuronal and glial cellular components are secreted in EVs from different animal models and human stem cells. The myelin proteolipid protein (PLP) and its spliced isoform DM20 are secreted by oligodendrocytes (glial cells that synthetize and assemble CNS myelin) and are also detected in EVs isolated from rodent brains[8,9]. Although PLP is the most abundant protein in CNS myelin in postnatal and adult brains, it is also expressed during embryonic stages, *i.e.* long before myelin is synthetized and assembled[10–12]. Currently, little is known about the association between PLP and EVs in humans, as well as whether its spatiotemporal expression pattern has any biological significance during early neurodevelopment[13].

[1]Centro de Investigación en Medicina Traslacional "Severo R. Amuchástegui" (CIMETSA), Instituto Universitario de Ciencias Biomédicas de Córdoba (IUCBC), Consejo Nacional de Investigaciones Científicas y Técnicas (CONICET), Av. Naciones Unidas 420, Barrio Parque Vélez Sarsfield, X5016KEJ Córdoba, Argentina. [2]Malena Herrera Lopez and Matías Bertone Arolfo have contributed equally to this work. ✉email: alfredo.caceres@iucbc.edu.ar; ana.moyano@iucbc.edu.ar

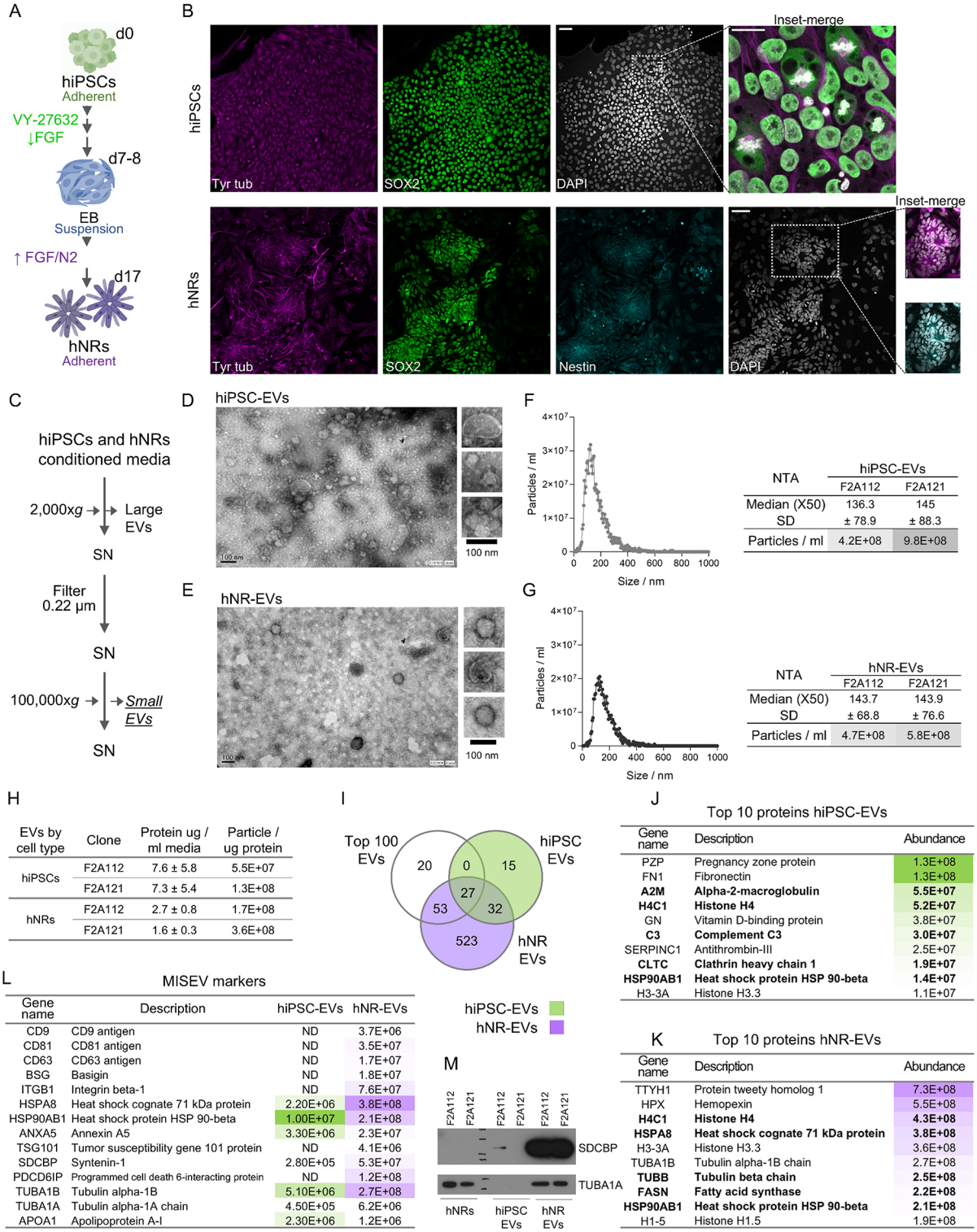

NTA	hiPSC-EVs	
	F2A112	F2A121
Median (X50)	136.3	145
SD	± 78.9	± 88.3
Particles / ml	4.2E+08	9.8E+08

NTA	hNR-EVs	
	F2A112	F2A121
Median (X50)	143.7	143.9
SD	± 68.8	± 76.6
Particles / ml	4.7E+08	5.8E+08

EVs by cell type	Clone	Protein ug / ml media	Particle / ug protein
hiPSCs	F2A112	7.6 ± 5.8	5.5E+07
	F2A121	7.3 ± 5.4	1.3E+08
hNRs	F2A112	2.7 ± 0.8	1.7E+08
	F2A121	1.6 ± 0.3	3.6E+08

Gene name	Description	Abundance
PZP	Pregnancy zone protein	1.3E+08
FN1	Fibronectin	1.3E+08
A2M	**Alpha-2-macroglobulin**	**5.5E+07**
H4C1	**Histone H4**	**5.2E+07**
GN	Vitamin D-binding protein	3.8E+07
C3	**Complement C3**	**3.0E+07**
SERPINC1	Antithrombin-III	2.5E+07
CLTC	**Clathrin heavy chain 1**	**1.9E+07**
HSP90AB1	**Heat shock protein HSP 90-beta**	**1.4E+07**
H3-3A	Histone H3.3	1.1E+07

Gene name	Description	Abundance
TTYH1	Protein tweety homolog 1	7.3E+08
HPX	Hemopexin	5.5E+08
H4C1	**Histone H4**	**4.3E+08**
HSPA8	**Heat shock cognate 71 kDa protein**	**3.8E+08**
H3-3A	Histone H3.3	3.6E+08
TUBA1B	Tubulin alpha-1B chain	2.7E+08
TUBB	**Tubulin beta chain**	**2.5E+08**
FASN	**Fatty acid synthase**	**2.2E+08**
HSP90AB1	**Heat shock protein HSP 90-beta**	**2.1E+08**
H1-5	Histone H1.5	1.9E+08

Gene name	Description	hiPSC-EVs	hNR-EVs
CD9	CD9 antigen	ND	3.7E+06
CD81	CD81 antigen	ND	3.5E+07
CD63	CD63 antigen	ND	1.7E+07
BSG	Basigin	ND	1.8E+07
ITGB1	Integrin beta-1	ND	7.6E+07
HSPA8	Heat shock cognate 71 kDa protein	2.20E+06	3.8E+08
HSP90AB1	Heat shock protein HSP 90-beta	1.00E+07	2.1E+08
ANXA5	Annexin A5	3.30E+06	2.3E+07
TSG101	Tumor susceptibility gene 101 protein	ND	4.1E+06
SDCBP	Syntenin-1	2.80E+05	5.3E+07
PDCD6IP	Programmed cell death 6-interacting protein	ND	1.2E+08
TUBA1B	Tubulin alpha-1B	5.10E+06	2.7E+08
TUBA1A	Tubulin alpha-1A chain	4.50E+05	6.2E+06
APOA1	Apolipoprotein A-I	2.30E+06	1.2E+06

Here we show that hiPSCs and hNRs secrete EVs (hiPSC-EVs and hNR-EVs, respectively) enriched in proteins associated with EVs. Only hNR-EVs are enriched in neuronal and glial cellular components involved in CNS and neurite development, typically expressed at different developmental stages both *in vitro* and in human samples. Interestingly, hNR-EVs induce morphological changes in stem cells and a significant increase in neurite length in human and murine neurons. Both are associated with a significant dysregulation of SOX2 levels, a transcription factor that modulates neural differentiation and pluripotency. Remarkably, these effects were inhibited by antibodies against PLP, an unexpected cargo of hNR-EVs. In conclusion, our findings suggest that hNR-EVs, along with their molecular cargoes, might participate as trophic effectors during human neurodevelopment.

◀**Fig. 1**. **hiPSCs and hNRs cell culture**. (**A**) hiPSCs cultures and differentiation into hNRs to obtain conditioned media for EVs isolation. (**B**) Confocal micrographs and immunocytochemistry of hiPSCs and hNRs stained with antibodies against tyrosinated tubulin (Tyr tub, magenta), SOX2 (green) and nestin (cyan). DAPI (grayscale). Scale bars: hiPSCs 50 µm (10x) and inset 20 µm (63x). hNRs 50 µm (20x) and inset 20 µm (20x). **hiPSC-EVs and hNR-EVs characterization.** (**C**) Isolation of small EVs by differential ultracentrifugation. SN: supernatant. Representative TEM micrographs of hiPSC-EVs (**D**) and hNR-EVs (**E**). Size distribution by NTA of hiPSC-EVs (**F**) and hNR-EVs (**G**) showing particle concentration and median size distribution (X50). Data: mean ± SD. EVs were isolated from 3 to 6 plates of clones F2A112 and F2A121. 2 independent experiments (n = 2 per clone). (**H**) Protein levels (µg/ml media) and particle to protein ratio in hiPSC-EVs and hNR-EVs. Data: mean ± SD. EVs were isolated from 3 to 6 plates of clones F2A112 and F2A121 (n = 4-6 clone). **hiPSC-EVs and hNR-EVs are enriched in EV-related proteins.** (**I**) Venn diagram illustrating the overlap between the top 100 EVs proteins (Vesiclepedia) and those identified in hiPSC-EVs (light green) and hNR-EVs (light purple) by MS analysis. EVs were isolated from 3 to 6 plates of clones F2A112 and F2A121 (n = 2 per clone). Top 10 proteins identified in hiPSC-EVs (**J**) and hNR-EVs (**K**). Highlighted proteins are common to the top 100 EVs, hiPSC-EVs and hNR-EVs. (**L**) Abundance of EVs markers (transmembrane and cytosolic proteins) described by MISEV 2018 and apolipoprotein A-1 as contaminant. (**M**) Western blot analysis of SDCBP (Syntenin-1) and TUBA1A levels in protein extracts from hNRs (cell lysate) and EVs isolated from 3 to 6 plates of clones F2A112 and F2A121 (n = 1 per clone). Original blots are provided in Supplementary Fig. S2.

Results

Cell culture model and EVs characterization

Human induced pluripotent stem cells (hiPSCs) were differentiated into neural rosettes (hNRs) and characterized by immunofluorescence (Fig. 1A and B). hiPSCs colonies displayed their typical morphology expressing the pluripotency markers SOX2, NANOG and Oct3/4. hNRs showed radially-organized cells expressing SOX2 and the neural stem cell marker nestin (Fig. 1B and S1). EVs were isolated by ultracentrifugation from serum-free conditioned media from hiPSCs and hNRs (Fig. 1C). EVs' morphology and size distribution were evaluated using transmission electron microscopy (TEM) and nanoparticle track analysis (NTA). By TEM we found that hiPSC-EVs and hNR-EVs exhibit their canonical morphology (Fig. 1D and E). Size distribution by NTA showed that 50% of hiPSC-EVs and hNR-EVs are smaller than 145 nm with slight differences in particle concentration among different clones (Fig. 1F and G). These results showed that hiPSCs and hNRs secrete EVs with a homogeneous size distribution and particle concentration.

hiPSC-EVs and hNR-EVs are associated with EVs markers

To further characterize hiPSC-EVs and hNR-EVs we analyzed their protein composition by mass spectrometry (MS). hiPSC-EVs showed significantly higher levels of total protein content compared with hNR-EVs with similar particle to protein ratio[14,15] (Fig. 1H). MS analysis identified 74 proteins in hiPSC-EVs and 635 in hNR-EVs (Table S1). Compared with the top 100 proteins associated with EVs from the database Vesiclepedia[16], we found 27 proteins overlapping with hiPSC-EVs and 80 with hNR-EVs (Fig. 1I, Table S1). Some of them are among the top 10 proteins detected in hiPSC-EVs and hNR-EVs (Fig. 1J and K). Also, both preparations are enriched in MISEV markers[14,17] with only apolipoprotein A-1 as contaminant (Fig. 1L). Collectively, these results showed that our preparations are enriched in EVs markers and hNR-EVs exhibit a more complex protein signature compared with hiPSC-EVs.

hNR-EVs are associated with neuronal and glial cellular components

Gene ontology (GO) enrichment analysis with proteins from hiPSC-EVs and hNR-EVs revealed diverse terms among the top 10 significantly enriched in molecular functions (MF), cellular components (CC) and biological processes (BP) (Fig. S1). GO analysis indicated that 85% of proteins identified in hiPSC-EVs and 63% in hNR-EVs are associated with EVs. The distribution of proteins in both types of EVs showed similar proportions of proteins localized within the cytoplasm, plasma membrane, and endomembrane system (Fig. 2A). Both preparations showed a significant enrichment in filtered GO terms related to EVs in CC and BP (Fig. 2B and C). Furthermore, filtered GO terms related to neuronal and glial CC and BP categories were significantly enriched almost exclusively in hNR-EVs (Fig. 2D and E). Interestingly, hNR-EVs protein signature exhibits unique and overlapping proteins related to GO terms CNS development, neurite development and myelin sheath (Fig. 2F, Table S1). Among common proteins we found ITGB1, CNP, HSP90AA1 and unexpectedly PLP, the most abundant protein in CNS myelin (Fig. 2G). These results indicate that both preparations exhibit proteins associated with EVs and different subcellular localizations. Moreover, only hNR-EVs contain neuronal and glial proteins related to CNS development and remarkably to myelin sheet (myelination is a postnatal process).

In silico analyses: hNR-EVs proteins are expressed during neurodevelopment

To further confirm that hNRs express CNP, HSP90AA1, ITGB1 and PLP under different culture conditions, *i.e.* cell source and protocol of differentiation, we analyze RNAseq datasets from 3D hiPSC-derived neural spheroids[18] and hNRs derived from human embryonic stem cells (hESCs)[19]. We found that CNP, HSP90AA1, ITGB1 and PLP are expressed at different time points, culture conditions and cell types (Fig. 3A and B). Moreover, scRNAseq datasets using UCSC Cell Browser[20] showed that their transcripts are expressed in hiPSC-derived brain organoids[21] and human fetal brain[22] at various stages during neurodevelopment (Fig. 3C). Similar results were observed at the protein level in MS datasets from fetal human brain[23] (Fig. 3D). These observations

G

hNR-EVs proteins common to CNS development, neurite development and myelin sheet

GO term	Gene name	Description	Abundance
CNS development Neurite development Myelin sheet	CNP	2',3'-cyclic-nucleotide 3'-phosphodiesterase	2.3E+06
	HSP90AA1	Heat shock protein HSP 90-alpha	2.2E+07
	ITGB1	Integrin beta-1	7.6E+07
	PLP	Myelin proteolipid protein	7.1E+06
CNS development Neurite development	CDC42	Cell division control protein 42 homolog	2.0E+06
	CTNNA1	Catenin alpha-1	1.7E+06
	CTNNB1	Catenin beta-1	1.9E+06
	DMD	Dystrophin	4.6E+06
	DPYSL2	Dihydropyrimidinase-related protein 2	1.5E+07
	HSP90AB1	Heat shock protein HSP 90-beta	2.1E+08
	IGF2BP1	Insulin-like growth factor 2 mRNA-binding protein 1	5.7E+05
	NCKAP1	Nck-associated protein 1	1.1E+06
	NGFR	Tumor necrosis factor receptor superfamily member 16	ND
	PAFAH1B1	Platelet-activating factor acetylhydrolase IB subunit beta	7.2E+05
	PHGDH	D-3-phosphoglycerate dehydrogenase	1.7E+07
	PLXNB2	Plexin-B2	1.1E+06
	RTN4	Reticulon-4	1.1E+06
	SYT1	Synaptotagmin-1	7.2E+05
	VIM	Vimentin	9.2E+06
	YWHAH	14-3-3 protein eta	1.2E+06
CNS development Myelin sheet	CALM3	Calmodulin-3	2.1E+06

Fig. 2. hiPSC-EVs and hNR-EVs are enriched in proteins related to EVs. (**A**) Protein distribution as percentage of total proteins detected by MS in hiPSC-EVs (74 proteins) and hNR-EVs (635 proteins). Proteins are categorized based on GO analysis of their cellular localization: cytoplasm (GO:0005737), plasma membrane (GO:0005886), endomembrane system (GO:0012505) and EVs (GO:1903561). (**B** and **C**) GO enrichment analysis showing the significance (-log10 of adjusted *p*-value) of GO terms associated with EV-related proteins in hiPSC-EVs (light green) and hNR-EVs (light purple) in CC and BP categories. **hNR-EVs are enriched in proteins related to neuronal and glial CC and BP.** (**D** and **E**) GO enrichment analysis highlighting neuronal- and glial-related CC and BP terms. (**F**) Venn diagram depicting the overlap between proteins identified by MS in hNR-EVs and their association with GO terms: CNS development (GO:0007417, light red), neurite development (GO:0010975, light blue) and myelin sheet (GO:0043209, light purple). (**G**) Proteins identified by MS in hNR-EVs common to CNS development, neurite development and/or myelin sheet.

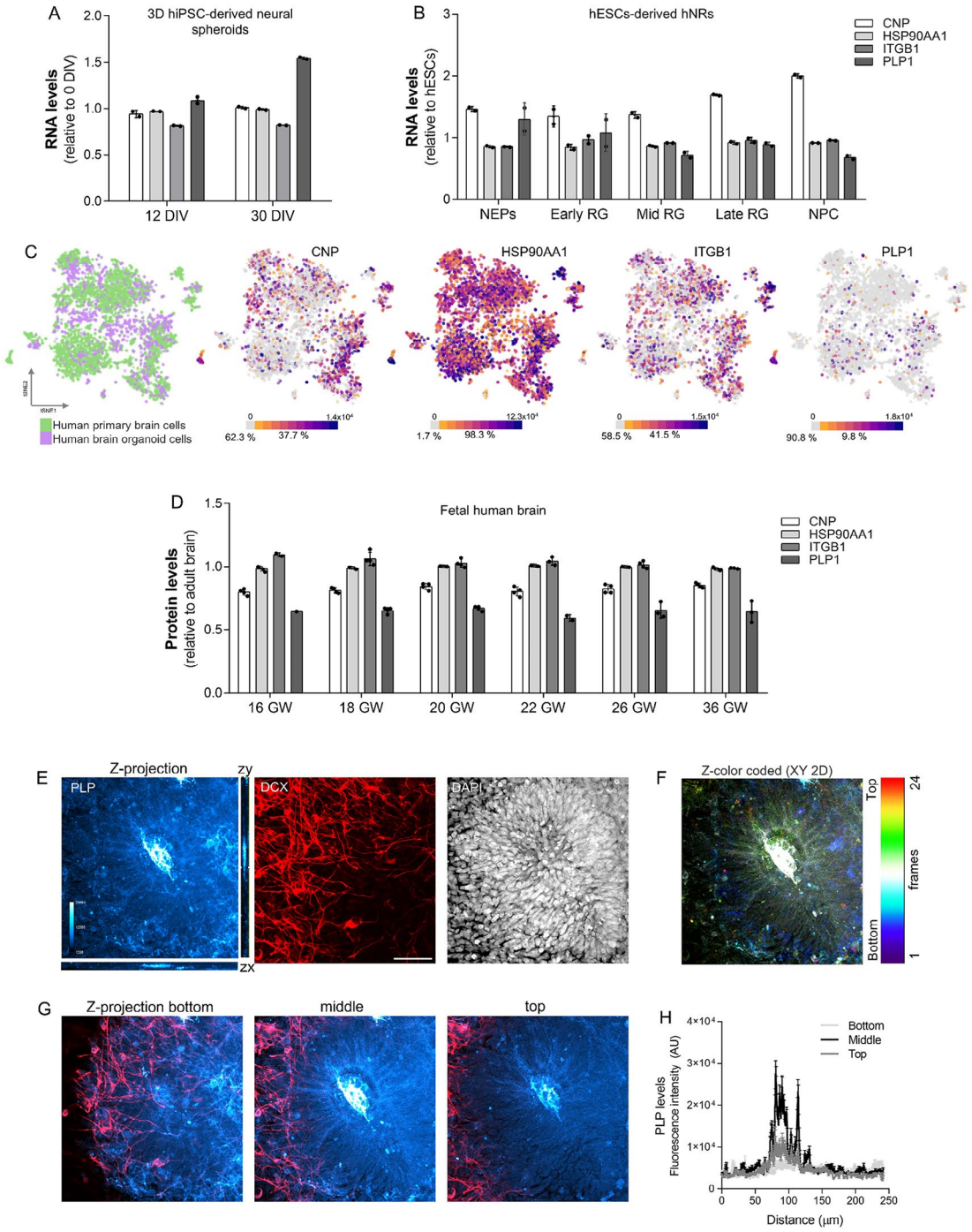

Fig. 3. **hNR-EVs proteins in hNRs, brain organoids and human brain.** (**A**) Expression of CNP, HSP90AA1, ITGB1 and PLP in RNAseq datasets from 3D hiPSC-derived neural spheroids at 12 and 30 days *in vitro* (DIV) relative to 0 DIV and (**B**) hNRs derived from human embryonic stem cells (hESCs) at different differentiation stages: neuroepithelial cells (NEPs), radial glia (RG), and neural progenitor cells (NPC). RNA levels are relative to undifferentiated hESCs. (**C**) tSNE plots showing the expression of CNP, HSP90AA1, ITGB1 and PLP in scRNA-seq datasets. Data includes human primary fetal brain cells (green-filled circle, n = 48, 10-24 postconceptual weeks [PCW]) and brain organoids (purplefilled circle, n = 31, 5-15 weeks, derived from 10 hiPSCs lines). (**D**) Protein levels of CNP, HSP90AA1, ITGB1 and PLP in fetal human brain samples (16, 18, 20, 22 and 36 gestational weeks [GW]) relative to adult human brain samples. **PLP has a differential cellular localization in hNRs.** (**E**) Confocal micrographs of hNRs stained with antibodies to PLP (cyan hot LUT) and DCX (red) showing maximum intensity projections of confocal Z-stacks and lateral sections. DAPI (grayscale). (**F**) Z-color coded XY 2D projections of confocal Z-stacks. (**G**) Transverse sections from bottom, middle and to top segments of hNRs. (**H**) PLP distribution in hNRs: quantification of fluorescence intensity (arbitrary units, AU) across transverse sections. Scale bar: 50 µm at 20x.

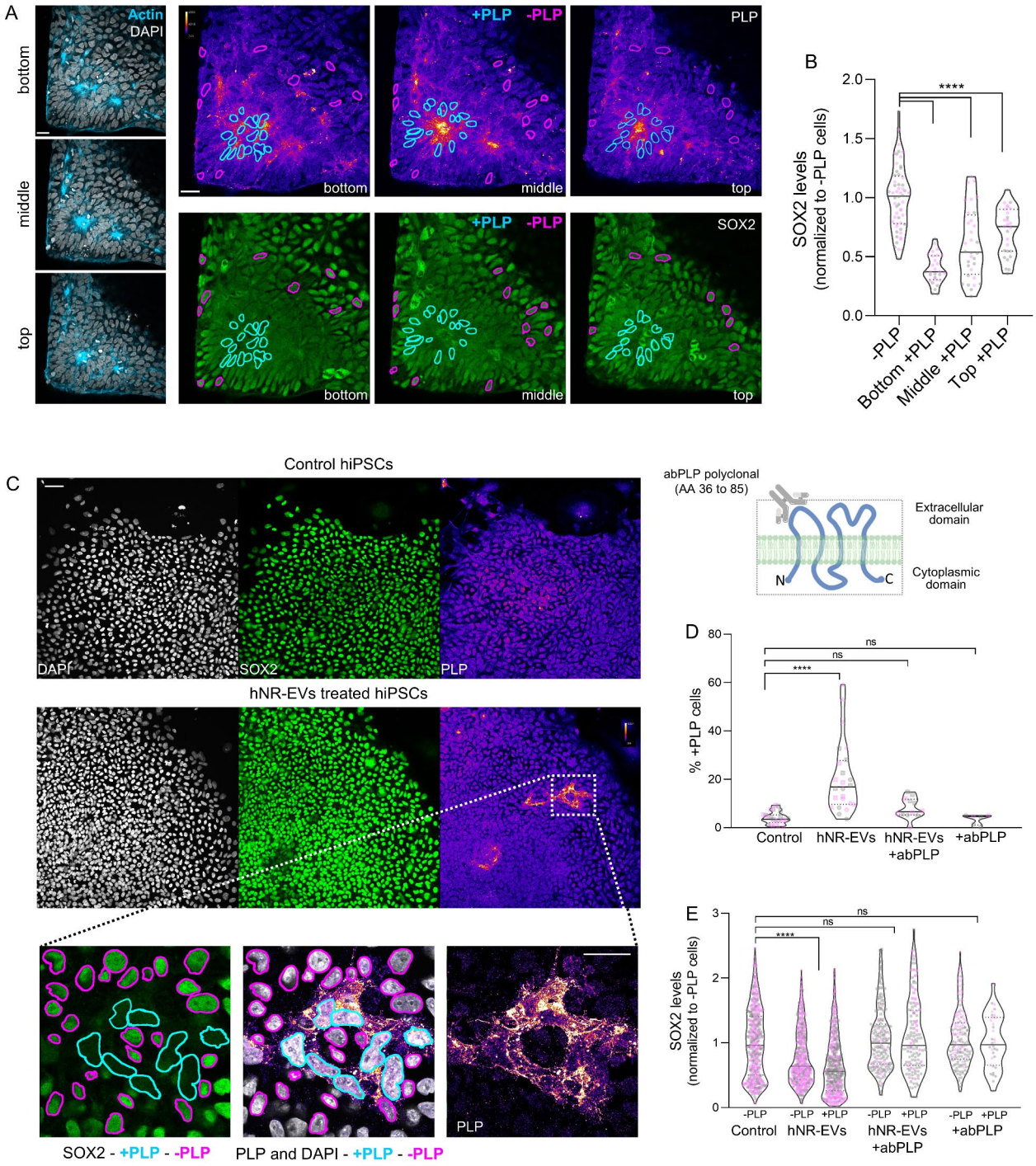

indicate that proteins associated with hNR-EVs, which are linked to CNS development and myelin sheath, are expressed at various stages during human brain development before myelination.

Cellular localization of PLP and biological activity of hNR-EVs

PLP-deficient mice exhibit dysfunctional EVs release and develop progressive axonal degeneration, however, the biological significance of PLP in human neurodevelopment remains unknown[9,24]. To validate the expression of PLP in hNRs we analyzed by immunofluorescence its cellular distribution in hiPSCs and hNRs. We found that PLP exhibits a radial and differential localization in hNRs outward from their central lumen (Fig. 3E-H) but is not expressed in hiPSCs (Fig. S1). Furthermore, hNRs +PLP cells distributed along the central lumen exhibited significantly lower SOX2 protein levels compared to -PLP cells (Fig. 4A and B). Since EVs secreted by stem cells can maintain pluripotency[25] we speculated that hNR-EVs might induce changes in stem cells. Thus, we probed this hypothesis by supplementing hiPSCs cultures with hNR-EVs. Consequently, after EVs treatment 20.8% hiPSCs switch into +PLP cells displaying a significant decrease in SOX2 protein levels (Fig. 4C-E). To evaluate

◀**Fig. 4. SOX2 has a differential distribution in hNRs.** (**A**) Confocal micrographs of hNRs stained with phalloidin (cyan) for actin, antibodies to PLP (Fire LUT) and SOX2 (green). Images represent transverse sections through the bottom, middle, and top segments of hNRs and selected -PLP (pink circle) and +PLP (sky-blue circle) cells. DAPI (grayscale). Scale bar 20 µm at 63x. (**B**) Violin plot showing the normalized SOX2 fluorescence intensity distribution in -PLP and +PLP cells. Each point represents a cell derived from F2A112 (gray-filled circle) and F2A121 (pink-filled circle) clones (n = 1 per clone). One-way ANOVA followed by Tukey's test. ****$p < 0.0001$. **Biological activity of hNR-EVs in stem cells.** (**C**) Confocal micrographs of hiPSCs untreated (control) and treated with hNR-EVs, stained with antibodies to PLP (Fire LUT) and SOX2 (green). Insets show -PLP (pink circle) and +PLP (sky-blue circle) cells. DAPI (grayscale). Scale bar: 50 µm at 20 × and 25 µm at 63 × for insets. (**D**) Violin plot of the percentage of +PLP distribution in untreated (control) or treated cells with hNR-EVs, hNR-EVs incubated with anti-PLP antibodies (hNR-EVs + abPLP) and anti-PLP antibodies (abPLP). Each point represents a field. hiPSCs and EVs derived from F2A112 (gray-filled circle) and F2A121 (pink-filled circle) clones (n = 2-3 per clone, represented by ○, △ and □; 15-130 cells per field). (**E**) Violin plot showing the normalized SOX2 fluorescence intensity distribution in -PLP and +PLP cells under control or treated conditions. Each point represents a cell. Data from hiPSCs and EVs derived from F2A112 (gray-filled circle) and F2A121 (pink-filled circle) clones (n = 2-3 per clone, represented by ○, △ and □; 15-80 cells per field). Panels D and E: Kruskal-Wallis test followed by Dunn's test. ****$p < 0.0001$ and ns: not significant.

a potential contribution of PLP to this phenotype, we examined whether antibodies targeting an extracellular topological domain of PLP (amino acids 36-85) might inhibit hNR-EVs bioactivity[9,26]. Accordingly, the treatment with anti-PLP antibodies significantly reduced +PLP cells and restored SOX2 protein levels (Fig. 4D and E). These findings collectively support the idea that hNRs express PLP and suggest that hNR-EVs induce changes in stem cells homeostasis, which is restored by blocking with antibodies targeting an extracellular domain of PLP.

Contribution of hNR-EVs to neurite extension

To study hNR-EVs biological activity in neurite development, we supplemented human and rat cultured neurons with EVs to evaluate their contribution to neuritic and axonal growth. Whilst human neurons were obtained by hiPSCs differentiation, rat neurons were isolated from embryonic rat brain hippocampi (E18.5)[27,28]. In this context, only hNR-EVs treatment promoted neuritic extension of human hiPSC-derived neurons at 2 DIV, paralleled by a significant increase in SOX2 levels compared with control and hiPSC-EVs treated cells (Fig. 5A-D). Moreover, hNR-EVs incubation with anti-PLP antibodies significantly restored neurite length and SOX2 to control levels (Fig. 5C and D). Importantly, 2 DIV human neuronal cultures are still enriched in stem cells (Fig. 5A, arrowheads). Treatment with hNR-EVs did not dysregulate SOX2 levels in stem cells or the number of neurons compared with control cells (Fig. S2). Similar results were observed in embryonic hippocampal rat neurons in culture. Accordingly, hNR-EVs treatment induced an increase in total neuritic length at 1 DIV, displaying a significant dysregulation of SOX2 levels (Fig. 5E-G). Moreover, hNR-EVs also increased the population of polarized neurons (+Tau1) at 1 DIV (Fig. 5H), suggesting a role in cultured neurons development. In addition, these effects were restored by incubating hNR-EVs with anti-PLP antibodies (Fig. 5E-H). Collectively, these results support the hypothesis that hNR-EVs not only remodel stem cells homeostasis but also enhance the growth of cultured CNS neurons through a PLP-mediated mechanism.

Discussion

Cell culture models obtained by hiPSC differentiation can recapitulate human neural tube formation. Emerging evidence indicates that EVs are key players to shape human CNS development at the molecular and cellular level. In this work, we show that hNR-EVs are enriched in neuronal and glial proteins involved in CNS development, usually expressed along different cellular stages and cell types in human neurodevelopment. Remarkably, hNR-EVs stimulate morphological changes in stem cells and neurons, promoting neuritic extension in human and rat neuronal models. These effects were associated with a significant dysregulation of SOX2 and inhibited by an antibody-dependent blockade of the extracellular domain of PLP, an unexpected neuroglial cargo present in hNR-EVs. In summary, our data supports the idea that hNRs secrete bioactive EVs containing neural components, exhibiting trophic factor roles during early CNS development in human and murine cellular models.

Several works have focused on EVs secreted by neural stem and progenitor cells due to their potential regenerative effects in neurological disorders[5]. However, biological aspects behind EVs secreted during human neural tube formation and CNS development have been understudied[7]. Human iPSCs resemble the inner cell mass of the blastocyst and differentiate into hNRs characterized by an ensemble of neuroepithelial, stem and progenitor cells. Consistent with other studies[29,30], our proteomic analysis showed that the protein composition of hNR-EVs is more complex than hiPSC-EVs, which could potentially be linked to the richer cellular diversity of hNRs compared to hiPSCs. These findings indicate that proteins involved in CNS development are selective cargoes of hNR-EVs and might be defined by hNRs cellular and molecular composition.

PLP is the most abundant transmembrane protein in CNS myelin and is secreted by murine oligodendrocytes in EVs[8,9]. Although the biological significance of PLP carrying EVs is unclear, *PLP*$^{-/-}$ knockout mice exhibit impaired oligodendroglial EVs release and axonal transport[6,9]. Moreover, *in vitro* studies showed that at least a fragment of PLP can regulate oligodendrocyte proliferation[26]. In this work, we describe the presence of PLP in hNR-EVs, unveiling unreported biological contributions in maintaining stem cell homeostasis and neuritic extension of cultured neurons, which are selectively inhibited by anti-PLP antibodies. These observations

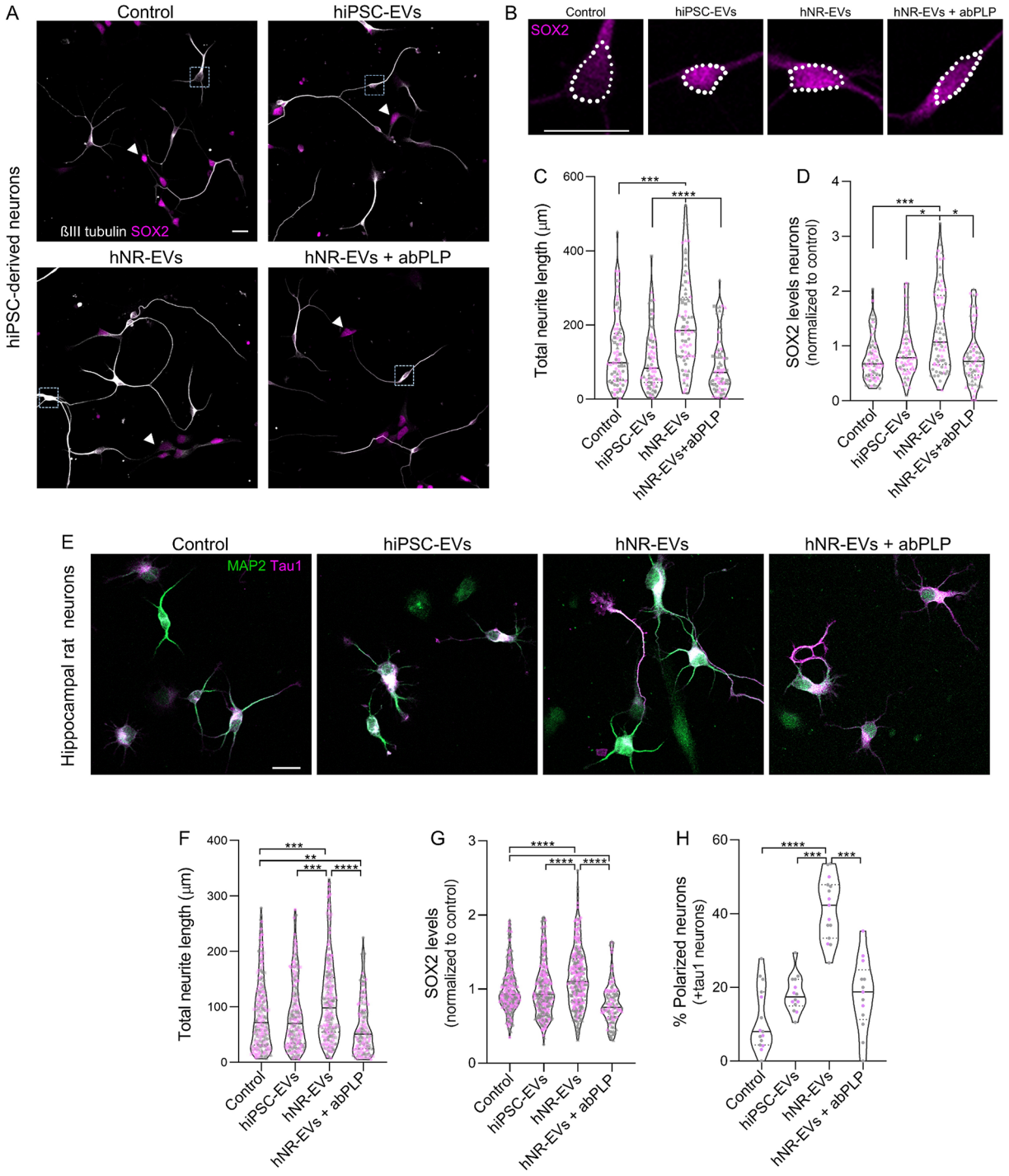

Fig. 5. **hNR-EVs induce neurite growth in human and murine neurons.** (**A**) Confocal micrographs of human neurons control and treated with hiPSC-EVs, hNR-EVs and hNR-EVs incubated with anti-PLP antibodies (hNR-EVs + abPLP) stained with antibodies to ß-III tubulin (grayscale) and SOX2 (magenta). (**B**) Inset from A in selected nuclei: SOX2 levels (magenta). Scale bar: 20 µm at 20x. (**C**) Violin plot of total neurite length distribution and (**D**) normalized SOX2 fluorescence intensity in control or treated conditions. Each point represents a cell. Data from EVs derived from F2A112 (gray-filled circle) and F2A121 (pink-filled circle) clones (n = 2-3 per clone, represented by ○, △ and □; 10-25 cells per field). Kruskal-Wallis test followed by Dunn's test. Ns: no significant, $^{*}p < 0.05$, $^{***}p < 0.001$ and $^{****}p < 0.0001$. (**E**) Murine neurons stained with antibodies to MAP2 (green) and Tau1 (magenta) control and treated with hiPSC-EVs, hNR-EVs and hNR-EVs incubated with anti-PLP antibodies (hNR-EVs + abPLP). Scale bar: 20 µm at 20x. (**F**) Violin plot of total neurite length distribution, (**G**) normalized SOX2 fluorescence intensity (**H**) and polarized (+Tau1) neurons in control or treated conditions. Each point represents a cell (**F**, **G**) or a field (**H**). Data from EVs derived from F2A112 (gray-filled circle) and F2A121 (pink-filled circle) clones (n = 2-3 per clone, represented by ○, △ and □; 15-32 cells per field). Kruskal-Wallis test followed by Dunn's test. Ns: no significant and $^{**}p < 0.01$, $^{***}p < 0.001$ and $^{****}p < 0.0001$.

support the hypothesis that neural components associated with hNR-EVs could function as modulators of CNS development.

PLP and its spliced variant DM20 have been detected in embryonic cells capable of differentiating into neural cells, even before myelination[10,12,31]. Loss- and gain-of-function studies in animal models and PLP mutations associated with Pelizaeus-Merzbacher disease (PMD) highlight the importance of PLP in myelin's axon-supportive function[24,32,33]. PLP/DM20 induce the formation of vesicles and multilamellar assemblies that might influence EVs biogenesis[34,35]. Our findings suggest that PLP/DM20 might have a wider biological role during human CNS development beyond myelination and axonal support. Moreover, hNRs could provide a novel model to study the relevance of EVs biology in PMD and other neurodevelopmental disorders.

EVs exhibit a wide range of subtypes, each one transporting diverse molecular cargos, and their biological effects could be influenced by the cellular context of recipient cells[36]. The transcription factor SOX2 regulates pluripotency and neural specification by regulating gene expression[37] and stem-cell-derived EVs regulate SOX2 expression[38]. Our findings indicate that hNR-EVs can influence SOX2 levels, with effects differing between undifferentiated and differentiated cells. While our study did not directly investigate the mechanisms by which hNR-EVs might dysregulate SOX2, we hypothesize that a subset of hNR-EVs, particularly those inhibited by anti-PLP antibodies, may carry or induce upstream effectors. These observations suggest that EVs can impact CNS development by modulating SOX2 expression based on the environment of the recipient cells. Further research is needed to explore how hNR-EVs might affect different stem cell lineage trajectories and their biological effects at different timepoints during neuronal development.

Stem cells-derived EVs can regulate diverse biological mechanisms under physiological and pathological conditions, but their contribution to human CNS development is unknown[7]. In this regard, technical limitations related to EVs isolation or culturing human neurons and glial cells reproducibly, have hindered comprehensive studies to unveil their functional properties. Previous works have stated potential cross contaminations with coisolated nanoparticles during EVs isolation[14]. Although we cannot discard this possibility, our assays using anti-PLP antibodies support specific properties. Thus, further studies are needed to clearly discriminate the biological roles of EVs subtypes and their molecular cargoes during CNS development.

In summary, the data presented in this work supports the idea that hiPSCs and hNRs secrete EVs with different protein cargoes, being hNR-EVs specifically enriched in neural components. Remarkably, hNR-EVs induce changes through a cell context-dependent manner, influencing hiPSCs' phenotype but also neurite development of cultured neurons. Future studies will address the biological role of neural components associated with hNR-EVs, and their contribution to the development of human brain cells in health and disease.

Experimental procedures

hiPSCs cell culture and differentiation

2 hiPSCs clones (F2A112 and F2A121) from a healthy donor were obtained from PLACEMA Foundation where they were reprogrammed and characterized (supplementary note) under the approval of ethical committees and a written informed consent previously approved by the ethical board of the involved institutions[39]. To obtain hNRs we used a previously described protocol[27], with modifications. Briefly, hiPSCs were cultured on a layer of irradiated embryonic mouse fibroblasts (MEFi) in serum-free medium (Knockout serum replacement-KSR, Thermo Fisher, cat. # 10828028) in the presence of a ROCK inhibitor (Y-27632, Calbiochem, cat. # 688000) and the fibroblast growth factor (FGF, Peprotech, cat. # 688000). hiPSCs colonies were manually selected and enzymatically dissociated to be differentiated into embryoid bodies (EBs) in medium with Y-27632 and low FGF (4 ng/ml). Between 7 and 8 days in culture, media was supplemented with N2 (Thermo Fisher, cat. # 17502048) and FGF (20 ng/ml) and on day 10 EBs were adhered to the surface covered with Geltrex (Thermo Fisher, cat. # A1413301). After 4-5 days in culture, the area and thickness of the neural rosettes increased (definitive neuroepithelium). Human neurons were obtained according to Zhang and Zhang[27]. Briefly, neural rosettes were dissected and plated without substrate to generate neurospheres (cells in suspension). Neurospheres were dissociated with accutase (Thermo Fisher, cat. #A11105-01) and mechanically plated on surfaces treated with Poly-L-Lysine (Sigma-Aldrich, cat. #P2636) / Geltrex in media supplemented with: neurobasal (Thermo Fisher, cat. #21103049), N2, B27 (Thermo Fisher, cat. #17504044), Glutamax (Thermo Fisher, cat. #A1286001), NEAA (Thermo Fisher, cat. #11140050), BDNF (Peprotech, cat. #450-02), GDNF (Peprotech, cat. #450-10), ascorbic acid (Sigma-Aldrich, cat. #A4403), IGF-1 (Peprotech, cat. #100-11), and cAMP (Sigma-Aldrich, cat. #D0627). Media was changed every 2 days, replacing half of the initial media volume. Cell cultures in all stages were grown in defined culture medium to rule out the incorporation of EVs present in media supplemented with sera[40]. hiPSC- and hNR-conditioned media were collected every other day.

Primary culture of hippocampal neurons

Hippocampal neuronal cultures were prepared according to Wilson et al[28]. Briefly, hippocampi were isolated from embryonic rat brain of E18.5 days and enzymatically and mechanically dissociated. Neurons were plated in glass coverslips treated with poly-L-lysine (1 mg/ml) in DMEM supplemented with 10% horse serum. After 1 h the medium was replaced by Neurobasal culture medium supplemented with B27, Glutamax and antibiotics (penicillin and streptomycin). Animal procedures followed the Institutional Animal Care and Use Committee (CICUAL) and NIH guidelines. All procedures were approved by the CICUAL of Instituto de Investigación Médica Mercedes y Martin Ferreyra (INIMEC-CONICET-UNC).

Immunocytochemistry and confocal microscopy

Cells were fixed in 4% paraformaldehyde (PFA) at room temperature (RT) for 15 min and then washed 3 times with phosphate buffered saline (PBS). Then, they were permeabilized with PBS-Triton 0.25% and blocked for 1 h with bovine serum albumin 5% in PBS-Triton 0.1% at RT. Subsequently, some of the following primary antibodies

were incubated 24 h at 4 °C: rabbit anti-SOX2 (1:100 dilution, Abcam, ab137285), rabbit anti-NANOG (1:100 dilution, Santa Cruz Biotechnology, sc-33759), mouse anti-Oct3/4 (1:100 dilution, Santa Cruz Biotechnology, sc-5279) rabbit anti-doublecortin (DCX, 1:1000 dilution, Abcam, ab207175), mouse anti-tyrosinated tubulin (TUB-1A2, 1:1000 dilution, Sigma, T9028), chicken anti-nestin (1:500 dilution, Abcam, ab134017), mouse anti-ßIII tubulin (2G10, 1:1000 dilution, Abcam, ab78078), mouse anti-tau1 (clone CC1C6; 1:500 dilution, Millipore, MAB3420), chicken anti-MAP2 (1:500 dilution, Abcam, ab134017) and rat AA3 monoclonal hybridoma anti-proteolipid protein 1 (PLP, 1:100 dilution). AA3 was a kind gift of Dr. Irene Givogri and Dr. Ernesto Bongarzone. Next, the following secondary antibodies were incubated at RT for 1h: anti-IgG rabbit (1:1000; Alexa Fluor 488 or 546, Life Technologies, A11008 or A11010), anti-IgG mouse (1:1000 dilution, Alexa Fluor 546; Life Technologies, A11030), anti-IgY chicken (1:1000 dilution, Alexa Fluor 488; Invitrogen, A11039) and/or anti-IgG rat (dilution 1:1000, Alexa Fluor 568; Molecular Probes, A11077). Cell nuclei were labeled with DAPI (4',6-diamidino-2-phenylindole, Invitrogen, P36931). Images were obtained in the Zeiss LSM 800 Confocal Optical Microscope at the Centro de Micro y Nanoscopía de Córdoba (CEMINCO-CONICET-UNC) and analyzed using ImageJ image (NIH, Bethesda, MD). Neuronal morphological analysis was performed using ImageJ to measure total neurite length (sum all branches) in individual cells. Neurites were visualized using ßIII-tubulin antibodies for human neurons or MAP2 and Tau1 antibodies for murine neurons. The percentage of polarized murine neurons was determined by identifying +Tau1 neurites. Nuclear staining with DAPI was used for image thresholding and segmentation to identify nuclear areas. Nuclear area per cell was quantified using ImageJ particle analysis, and the resulting masks were applied to quantify SOX2 protein levels in hiPSCs, hNRs, and neurons. At least 3-4 images per condition were analyzed.

Isolation of hiPSC-EVs and hNR-EVs

EVs were isolated as described previously[41,42]. Briefly, cell culture conditioned media was collected from hiPSCs and hNRs (2-10 ml) and centrifuged at low speed (300 xg) to remove large particles. Supernatants were centrifuged 10 min at 2000 xg and then this supernatant filtered through a 0.22 µm filter. EVs were isolated after ultracentrifugation at 100,000 xg for 90 min. Isolated EVs were washed in 10 ml of PBS and pelleted again at 100,000 xg for 90 min. EVs were resuspended in 50 µl of 0.22-µm-filtered PBS. All centrifugation and ultracentrifugation steps were performed at 4 °C. hiPSC-EVs and hNR-EVs samples were stored at − 80 °C until further analysis.

Treatment of hiPSCs and neurons with hNR-EVs

Small hiPSCs colonies were plated in coverslips on a layer of MEFi in serum-free medium for 24 h before treatment. Human neurons were grown on coverslips for 24 h (1 DIV, days in vitro) and murine neurons for 1 h (0 DIV) before EVs treatment. Cells were treated with hiPSC-EVs or hNR-EVs isolated from 0.5 ml of conditioned media in a final volume of 0.5 ml serum-free medium and incubated 24 h at 37 °C. Antibody-mediated inhibition of hNR-EVs was performed with a commercial antibody that recognizes an extracellular topological domain of PLP at its N terminus (AA 36-85, Invitrogen, PA5-40788) incubating hNR-EVs with anti-PLP 1.25 ug/ml for 15 min before EVs treatment. After EVs supplementation, cells were fixed in 4% PFA for immunocytochemistry. hiPSCs were fixed 24 h after EVs supplementation. Human neurons were fixed at 2 DIV to recognize and analyse individual neurites, which are less distinguishable than at 5 DIV. Similarly, murine neurons were fixed at 1 DIV, as single neurites are less intertwined than at 3 DIV (Fig. S2A-C). At least two independent experiments were performed supplementing murine neurons, hiPSCs and human neurons derived from clones F2A112 and F2A121. In each experiment EVs were isolated from 3 to 6 plates of clones F2A112 and F2A121.

Electron microscopy and nanoparticle tracking analysis

hiPSC-EVs and hNR-EVs were fixed in 2% PFA and characterized by transmission electron microscopy (TEM) at the Centro de Microscopía Electrónica (INTA-CIAP) using the TEM Jeol 1200 EX II 14.33 electron microscope as previously described[42]. Nanoparticle tracking analysis (NTA) was performed using a ZetaView PMX-230 Twin Laser (Particle Metrix, Germany). Recordings were created by scanning 30 frames at 11 positions. Measurements parameters: maximum particle size at 1000 nm, minimum particle size at 10 nm, minimum brightness at 30, sensitivity at 80.0, shutter at 100 and cell temperature at 25 °C. Recording analyses were performed on ZetaView (version 8.05.16 SP7). NTA was performed at Instituto de Investigaciones en Microbiología y Parasitología Médica (IMPaM-UBA-CONICET).

Protein quantification

Proteins were measured by the bicinchoninic acid (BCA, Pierce, 23227) method. Using the EL800 BioTek microplate reader to determine the absorbance at 562 nm.

LC-MS analysis

Peptide separations were carried out on a nanoHPLC Ultimate3000 (Thermo Fisher) using a nano column EASY-Spray ES901 (15 cm × 50 µm ID, PepMap RSLC C18). The mobile phase flow rate was 300 nl/min using 0.1% formic acid in water (solvent A) and 0.1% formic acid and 100% acetonitrile (solvent B). The gradient profile was set as follows: 4-35% solvent B for 30 min, 35-90% solvent B for 1 min and 90% solvent B for 5 min. Two microliters of each sample were injected. MS analysis was performed using a Q-Exactive HF mass spectrometer (Thermo Fisher). For ionization, 1.9 kV of liquid junction voltage and 250 °C capillary temperature was used. The full scan method employed a m/z 375-1600 mass selection, an Orbitrap resolution of 120,000 (at m/z 200), a target automatic gain control (AGC) value of 3e6, and maximum injection times of 100 ms. After the survey scan, the 20 most intense precursor ions were selected for MS/MS fragmentation. Fragmentation was performed

with a normalized collision energy of 27 eV and MS/MS scans were acquired with a dynamic first mass, AGC target was 5e5, resolution of 30,000 (at m/z 200), intensity threshold of 4.0e4, isolation window of 1.4 m/z units and maximum IT was 200 ms. Charge state screening enabled to reject unassigned, singly charged, and equal or more than seven protonated ions. A dynamic exclusion time of 15 s was used to discriminate against previously selected ions. LC-MS analysis was performed at the Unidad de Espectrometría de Masa, Instituto de Biología Molecular y Celular de Rosario (UEM-IBR-CONICET).

MS data analysis

MS data were analyzed with Proteome Discoverer (version 2.4) (Thermo Fisher) using standardized workflows. Mass spectra *.raw files were searched against the database of Homo sapiens from Uniprot (UP000005640). Precursor and fragment mass tolerance were set to 10 ppm and 0.02 Da, respectively, allowing 2 missed cleavages, carbamidomethylation of cysteines as a fixed modification, methionine oxidation and acetylation N-terminal as a variable modification. Identified peptides were filtered using Percolator algorithm with a q-value threshold of 0.01.

GO enrichment analysis

MS datasets were used as input for GO enrichment analysis to detect potential molecular function, biological processes and cellular components GO terms using the g:Profiler2 (version e107_eg54_p17_bf42210)[43]. GO terms with g:SCS multiple testing correction method and a significance threshold of 0.05 were considered enriched. Enriched GO terms were visualized using Microsoft Excel (version 2212). GO subsets for EV-related proteins were selected with the following terms: extracellular vesicle, vesicle, vesicular, exosome and exosomal. GO subsets for neuronal- and glial-related proteins were selected with the following terms: neural, neuron, axon, glia, astrocyte, microglia, Schwann, oligodendrocyte, myelin, nervous, nerve, brain. Top 100 EVs proteins were used from Vesiclepedia[16] and Venn diagrams were created with https://molbiotools.com/listcompare.php.

In silico analyses

Gene Expression Omnibus (GEO) database freely archives and distributes public microarray, next-generation sequencing (NGS) results, and other forms of genomic data that can be combined and reanalyzed to reveal previously unknown relationships[44]. Using GEO repository, we analyze RNAseq datasets from 3D hiPSC-derived neural spheroids (GEO accession: GSE102139 from[18]) and hNRs derived from hESCs (GEO accession: GSE65369 from[19]). To analyze scRNAseq datasets we applied UCSC Cell Browser[20] with datasets from hiPSC-derived brain organoids (GEO accession: GSE124299 from[21]) and human fetal brain (Data available at dbGaP: phs000989.v3 from[22]). Data includes human primary fetal brain cells (n = 48, 10-24 postconceptual weeks [PCW]) and brain organoids (n = 31, 5-15 weeks, derived from 10 hiPSCs lines). The MS datasets were analyzed from PRIDE[45] datasets of human fetal and postnatal brain (Accession number: PXD004076 from[23]). Data includes human brain samples (16, 18, 20, 22 and 36 gestational weeks [GW] and adult postnatal).

Western blot

Samples were lysed with RIPA buffer (50 mM Tris-HCl pH 8, 1% v/v triton X-100, 1 mm EDTA and 0.15 M NaCl) and the protein concentration determined by BCA. The samples were diluted in Laemmli buffer (0.25% w/v Bromophenol Blue, 15% v/v ß-Mercaptoethanol, 50% v/v Glycerol, 10% w/v SDS and 0.25 M Tris-HCl pH 6, 8) and incubated at 95° C for 10 min. Lysates (5-10 µg protein) were resolved by sodium dodecyl sulfate 12% polyacrylamide gel electrophoresis (SDS-PAGE), at 200 V for 1 h (BioRad). Gels were transferred to a nitrocellulose or PVDF membrane at 100 V for 90 min at 4 °C. These membranes were incubated with a blocking solution (5% w/v non-fat dry milk diluted in TBS + 0.05% v/v Tween) for 1 h. After, incubated for 24 h at 4 C with the following primary antibodies: rabbit anti-syntenin 1 (1:2000 dilution, Abcam, ab133267) and mouse anti-tubulin α (1:2000 dilution, clone DM1A, Sigma, T9026). Membranes were washed 3 times with TBS-Tween 0.01% and incubated with peroxidase-labeled secondary antibodies to detect antibody reactivity by enhanced chemiluminescence (ECL).

Statistical analysis

Data was analyzed for normality using the Kolmogorov-Smirnov test. Comparisons were performed using the One-way ANOVA followed by Tukey's test or Kruskal-Wallis test followed by Dunn's multiple comparisons test. For all statistical analyses P values < 0.05 were considered significant. Outliers were identified by ROUT method and not included in the analyses. "n" refers to the number of independent experiments in each group. Data was examined and visualized using Microsoft Excel (version 2212), the GraphPad Prism 10.00 program (San Diego, California, www.graphpad.com). Violin plots show median (—) and quartiles (---).

Data availability

All processed data are available in the article and supporting information. The list of all proteins identified by mass spectrometry is included as Supporting information and raw data is available on request. Further details are available from the corresponding authors (A.L.M and A.C.) upon reasonable request.

Received: 16 September 2024; Accepted: 8 January 2025
Published online: 15 January 2025

References

1. Conti, L. & Cattaneo, E. Neural stem cell systems: Physiological players or in vitro entities?. *Nat. Rev. Neurosci.* **11**, 176–187 (2010).

2. Elkabetz, Y. & Studer, L. Human ESC-derived neural rosettes and neural stem cell progression. *Cold Spring Harb. Symp. Quant. Biol.* **73**, 377–387 (2008).
3. Mertens, J., Marchetto, M. C., Bardy, C. & Gage, F. H. Evaluating cell reprogramming, differentiation and conversion technologies in neuroscience. *Nat. Rev. Neurosci.* **17**, 424–437 (2016).
4. Van Niel, G., D'Angelo, G. & Raposo, G. Shedding light on the cell biology of extracellular vesicles. *Nat. Rev. Mol. Cell Biol.* **19**, 213–228 (2018).
5. Holm, M. M., Kaiser, J. & Schwab, M. E. Extracellular Vesicles: Multimodal envoys in neural maintenance and repair. *Trends Neurosci.* **41**, 360–372 (2018).
6. Schnatz, A., Müller, C., Brahmer, A. & Krämer-Albers, E. M. Extracellular Vesicles in neural cell interaction and CNS homeostasis. *FASEB BioAdv.* **3**, 577–592 (2021).
7. Bahram Sangani, N., Gomes, A. R., Curfs, L. M. G. & Reutelingsperger, C. P. The role of extracellular vesicles during CNS development. *Prog. Neurobiol.* **205**, 102124; 10.1016/j.pneurobio.2021.102124 (2021).
8. Krämer-Albers, E.-M. et al. Oligodendrocytes secrete exosomes containing major myelin and stress-protective proteins: Trophic support for axons?. *Proteom. Clini. Appl.* **1**, 1446–1461 (2007).
9. Frühbeis, C. et al. Oligodendrocytes support axonal transport and maintenance via exosome secretion. *PLoS Biol.* **18**, 1–28 (2020).
10. Timsit, S. et al. Oligodendrocytes originate in a restricted zone of the embryonic ventral neural tube defined by DM-20 mRNA expression. *J. Neurosci.* **15**, 1012–1024 (1995).
11. Spassky, N. et al. Single or multiple oligodendroglial lineages: a controversy. *Glia* **29**, 143–148 (2000).
12. Delaunay, D. et al. Early neuronal and glial fate restriction of embryonic neural stem cells. *J. Neurosci.* **28**, 2551–2562 (2008).
13. Kronquist, K. E., Crandall, B. F., Macklin, W. B. & Campagnoni, A. T. Expression of myelin proteins in the developing human spinal cord: Cloning and sequencing of human proteolipid protein cDNA. *J. Neurosci. Res.* **18**, 395–401 (1987).
14. Théry, C. et al. Minimal information for studies of extracellular vesicles 2018 (MISEV2018): A position statement of the International Society for Extracellular Vesicles and update of the MISEV2014 guidelines. *J. Extracell. Vesicles* **7**, 1535750; 10.1080/20013078.2018.1535750 (2018).
15. Webber, J. & Clayton, A. How pure are your vesicles?. *J. Extracell. Vesicles* **2**, 1–6 (2013).
16. Kalra, H. et al. Vesiclepedia: A compendium for extracellular vesicles with continuous community annotation. *PLOS Biol.* **10**, e1001450; 10.1371/journal.pbio.1001450 (2012).
17. Kugeratski, F. G. et al. Quantitative proteomics identifies the core proteome of exosomes with syntenin-1 as the highest abundant protein and a putative universal biomarker. *Nat. Cell Biol.* **23**, 631–641 (2021).
18. Simão, D. et al. Recapitulation of human neural microenvironment signatures in iPSC-derived NPC 3D differentiation. *Stem Cell Rep.* **11**, 552–564 (2018).
19. Edri, R. et al. Analysing human neural stem cell ontogeny by consecutive isolation of Notch active neural progenitors. *Nat. Commun.* **6**, 6500; 10.1038/ncomms7500 (2015).
20. Speir, M. L. et al. UCSC cell browser: Visualize your single-cell data. *Bioinformatics* **37**, 4578–4580 (2021).
21. Pollen, A. A. et al. Establishing cerebral organoids as models of human-specific brain evolution. *Cell* **176**, 743-756.e17 (2019).
22. Nowakowski, T. J. et al. Spatiotemporal gene expression trajectories reveal developmental hierarchies of the human cortex. *Science* **358**, 1318–1323 (2017).
23. Djuric, U. et al. Spatiotemporal proteomic profiling of human cerebral development. *Mol. Cell. Proteom.* **16**, 1558–1562 (2017).
24. Griffiths, I. et al. Axonal swellings and degeneration in mice lacking the major proteolipid of myelin. *Science* **280**, 1610–1613 (1998).
25. Hur, Y. H., Feng, S., Wilson, K. F., Cerione, R. A. & Antonyak, M. A. Embryonic stem cell-derived extracellular vesicles maintain ESC stemness by activating FAK. *Dev. Cell* **56**, 277-291 (2021).
26. Yamada, M., Ivanova, A., Yamaguchi, Y., Lees, M. B. & Ikenaka, K. Proteolipid protein gene product can be secreted and exhibit biological activity during early development. *J. Neurosci.* **19**, 2143–2151 (1999).
27. Zhang, X.-Q. & Zhang, S.-C. Differentiation of neural precursors and dopaminergic neurons from human embryonic stem cells. *Methods Mol. Biol.* **584**, 355–366 (2010).
28. Wilson, C., Rozés-Salvador V. & Cáceres A. Protocol protocol for evaluating neuronal polarity in murine models protocol for evaluating neuronal polarity in murine models. *STAR Protoc.* **1,** 100114; 10.1016/j.xpro.2020.100114 (2020).
29. Upadhya, R. et al. Extracellular vesicles from human iPSC-derived neural stem cells: miRNA and protein signatures, and anti-inflammatory and neurogenic properties. *J. Extracell. Vesicles* **9**, 1809064; doi.org/10.1080/20013078.2020.1809064 (2020).
30. Forero, A., Pipicelli, F., Maccarrone, G., Giaimo, R. D. & Cappello, S. Extracellular vesicle-mediated trafficking of molecular cues during human brain development. *Cell Rep.* **43,** 114755; 10.1016/j.celrep.2024.114755 (2024).
31. Campagnoni, A. T. & Skoff, R. P. The pathobiology of myelin mutants reveal novel biological functions of the MBP and PLP genes. *Brain Pathol.* **11**, 74–91 (2001).
32. Stadelmann, C., Timmler, S., Barrantes-Freer, A. & Simons, M. Myelin in the central nervous system: Structure, function, and pathology. *Physiol. Rev.* **99**, 1381–1431 (2019).
33. Nave, K. A. & Trapp, B. D. Axon-glial signaling and the glial support of axon function. *Ann. Rev. Neurosci.* **31**, 535–561 (2008).
34. Ruskamo, S. et al. Human myelin proteolipid protein structure and lipid bilayer stacking. *Cell. Mol. Life Sci.* **79**, 1–19 (2022).
35. Bizzozero, O. A. & Howard, T. A. Myelin proteolipid protein-induced aggregation of lipid vesicles: Efficacy of the various molecular species. *Neurochem. Res.* **27**, 1269–1277 (2002).
36. Gho, Y. S. & Lee, C. Emergent properties of extracellular vesicles: A holistic approach to decode the complexity of intercellular communication networks. *Mol. BioSyst.* **13**, 1291–1296 (2017).
37. Zhang, S. & Cui W. Sox2, a key factor in the regulation of pluripotency and neural differentiation. *World J. Stem Cells* **6**, 305-311 (2014).
38. Abedi, M., Hajinejad, M., Atabi, F. & Sahab-Negah, S. Exosome derived from human neural stem cells improves motor activity and neurogenesis in a traumatic brain injury model. *BioMed Res. Int.* **2022**, 6409346 (2022).
39. Casalia, M. L. et al. A familiar study on self-limited childhood epilepsy patients using hIPSC-derived neurons shows a bias towards immaturity at the morphological, electrophysiological and gene expression levels. *Stem Cell Res. Ther.* **12**, 590; 10.1186/s13287-021-02658-2 (2021).
40. Wiklander, O. P. B. et al. Extracellular vesicle in vivo biodistribution is determined by cell source, route of administration and targeting. *J. Extracell. Vesicles* **4**, 1–13 (2015).
41. Moyano, A. L. et al. Sulfatides in extracellular vesicles isolated from plasma of multiple sclerosis patients. *J. Neurosci. Res.* **94**, 1579–1587 (2016).
42. Thery, C. et al. Isolation and characterization of exosomes from cell culture supernatants. *Curr. Protoc. Cell Biol. Chapter* **3**, 1–29 (2006).
43. Raudvere, U. et al. G:Profiler: A web server for functional enrichment analysis and conversions of gene lists (2019 update). *Nucleic Acids Res.* **47**, W191–W198 (2019).
44. Edgar, R. Gene expression omnibus: NCBI gene expression and hybridization array data repository. *Nucleic Acids Res.* **30**, 207–210 (2002).
45. Perez-Riverol, Y. et al. The PRIDE database resources in 2022: A hub for mass spectrometry-based proteomics evidences. *Nucleic acids Res.* **50**, 543–552 (2022).

Acknowledgements
The authors would like to thank Dr. Cecilia Sampredo, Dr. Carlos Mas and Dr. Gonzalo Quassollo at CEMINCO-CONICET-UNC for their support with confocal analysis. Dr. Claudia Nome and Dr. Valeria Quevedo at IPAVE-CIAP-INTA for their support with TEM analysis. Dr. Soledad Bazán at CIQUIBIC-CONICET-UNC for her support with DLS analysis. Dr. Eduardo Ceccarelli, Dr. Germán Rosano and Lic. Alejo Cantoia at UEM-IBR-CONICET for their support with MS analysis. Dr. Marcela Cucher and Dr. María Eugenia Santana at IMPaM-UBA-CONICET for their support with NTA analysis. Cr. Candy Bravo and Cr. Pedro Bravo at FUCIBICO for grants management.

Author contributions
C.W., A.C. and A.L.M. designed the study. M.H.L., M.B.A., M.R., L.G., C.W., G.G.G., D.C. and A.L.M. performed experiments and analyzed data. ALM wrote the original draft. M.H.L., M.B.A., M.R., L.G., C.W., G.G.G., D.C., A.C.G., A.C. and A.L.M. reviewed and edited manuscript. C.W., A.C.G., A.C. and A.L.M. acquired funding. C.W., A.C.G., A.C. and A.L.M. provided resources and materials. A.C. and A.L.M. supervised study.

Funding
This work was supported by the International Society for Neurochemistry (ISN CAEN "Return Home Grant" to ALM) by the Consejo Nacional de Investigaciones Científicas y Técnicas (CONICET, PIP 11220200102807CO to C.W., A.L.M., A.C.G. and A.C.) and the Agencia Nacional de Promoción Científica y Tecnológica (ANPCYT, PRESTAMO BID PICT 2019/00236 to A.L.M.). M.H.L., M.R., C.W., G.G.G., D.C., A.C.G., A.C. and A.L.M. are investigators of CONICET.

Competing interests
The authors declare no competing interests.

Additional information
Supplementary Information The online version contains supplementary material available at https://doi.org/10.1038/s41598-025-86094-9.

Correspondence and requests for materials should be addressed to A.C. or A.L.M.